Supplementary information

Anion-promoted CB[6] macromolecules dissolution for stable Zn-ion batteries

Xiaodong Yang,[#] Yuwei Zhao,[#] Shuangkun Lv, Leheng Zhong, Chencheng Yue, Shuai Zhan, Linwei Zhao, Chunfang Wang, Xuejin Li, Xiaoya Liu, Zijie Tang, Chunsun Zhang,* Chunyi Zhi, * Haiming Lv (Lyu) *

X. Yang, X. Liu, C. Zhang

MOE Key Laboratory of Laser Life Science & Institute of Laser Life Science, College of Biophotonics, South China Normal University, Guangzhou 510631, China

E-mail: zhangcs@scnu.edu.cn (C. Zhang)

Y. Zhao, C. Zhi, H. Lv

Department of Materials Science and Engineering, City University of Hong Kong

83 Tat Chee Avenue, Kowloon, Hong Kong 999077, China

E-mail: cy.zhi@cityu.edu.hk (C. Zhi); haimilyu@cityu.edu.hk (H. Lv (Lyu))

X. Yang, Y. Zhao, L. Zhong, C. Yue, S. Zhan, L. Zhao, C. Wang, S. Lv, Z. Tang, H. Lv, C. Zhi

Songshan Lake Materials Laboratory, Dongguan, Guangdong 523808, China

X. Li

State Key Laboratory of Heavy Oil Processing, School of Materials Science and Engineering, China University of Petroleum, Qingdao 266580, P. R. China

#These authors contributed equally

Experimental section

Material synthesis

Materials: glycoluril, $ZnSO_4 \cdot 7H_2O$ were purchased from Aladdin.

Electrolyte preparation: CB[6] added $ZnSO_4$ electrolyte was achieved by adding certain amount of CB[6] additives to the 1mol L^{-1} $ZnSO_4$, with the ratio of CB[6] to the total mixed electrolyte volume ranging from 0 to 5mM, 10mM, and 15mM, and the corresponding electrolytes were named as ZSO, 5 mM CB[6]/ZSO, 10 mM CB[6]/ZSO and 15 mM CB[6]/ZSO（5CB[6]/ZSO, 10CB[6]/ZSO and 15CB[6]/ZSO）.

Synthesis of CB[6]: Synthesis of cucurbit[n]uril was carried out according to the reported procedure by Kim et al[1]. A mixture of glycoluril (5.68 g, 40.0 mmol), formaldehyde (37% in water, 7.0 mL, 91 mmol), and 9 M sulfuric acid (20 mL) was heated at 75℃ for 24 h and then at 100℃ for 12 h. After the reaction mixture was poured into water (200 mL), acetone (1.0 L) was added to produce a precipitate. The precipitate was separated by decantation, washed with water/acetone (1:4), and filtered. The major product CB[6] was separated from the mixture by the fractional dissolution of other CB homologues with acetone/water (1:2).

Preparation of polyaniline (PANI): 0.2 mL aniline was added into 40 mL HCl (1.0 M) solution, and 200 mg ammonium persulfate was dissolved into another 40 mL HCl (1.0 M) solution. Both aniline and ammonium persulfate solutions were pre-cooled in an ice bath for 30 min. After that, the ammonium persulfate solution was added into the aniline solution dropwise with constant magnetic stirring under an ice bath. Following 6 h

magnetic stirring, the dark green PANI was filtrated and washed with deionized water three times. The collected PANI was freeze-dried overnight to obtain PANI powder[2].

Preparation of electrodes and assembly of full cells: The cathode electrodes were fabricated by mixing the active materials (PANI) with super P and polyvinylidene fluoride (PVDF) with a weight ratio of 6:3:1. The above mixture was mixed in an appropriate amount of N-methyl2-pyrrolidone (NMP) to form a slurry under vigorously stirring for 8 h, and then spread onto carbon cloth, dried in a vacuum oven at 60 °C overnight. The mass loading of the active materials was about 1-1.5 mg cm^{-2} . Symmetric cells and full cells were assembled using Zn foils (thickness-100 um) as anodes in CR-2032 coin cells, and 100 μL of electrolyte (1M $ZnSO_4$ or CB[6]/$ZnSO_4$) was utilized with the glass fiber (Waterman, grade GF/A) as the separator.

Electrochemical testing

The battery performance was evaluated by using CR2032 coin-type cells on a Neware BTS4000 battery test system. The Zn plating/stripping tests were performed on Zn symmetrical cells in the electrolytes with and without CB[6]. Coulombic efficiency (CE) measurements were performed on asymmetrical Cu||Zn cells. The corrosion, diffusion and hydrogen evolution behaviors of Zn foil electrode were performed under an electrochemical workstation (CHI 760e) with a three-electrode system (Zn foil as work electrode, Pt as counter electrode, and Ag/AgCl as reference electrode). The Tafel plots were measured by scanning between -0.8 V and -1.2 V at 1 mV s^{-1} . The diffusion curves were recorded by the chronoamperometry method under an overpotential of -

150 mV. The hydrogen evolution performance was collected through linear sweep voltammetry (LSV) with a potential range of -0.3 ~ 3 V at a scan rate of 1 mV s^{-1} . Electrochemical impedance spectroscopy (EIS) was implemented within a range of 10^5 to 10^{-1} Hz. The full cells were cycled between 0.3 and 1.6 V vs. Zn/Zn^{2+}, and the specific capacities were evaluated according to the mass of active materials.

The DOD was calculated by the area-specific capacity of discharge (1.62 mAh cm^{-2})/58.5 mAh cm^{-2} (theoretical area-specific capacity of Zn). In this case, theoretical area-specific capacity of Zn foil is 58.5 mAh cm^{-2} calculated by the following equation[3]:

$$C_t = \rho \times l \times m_c$$

Where C_t represents the theoretical capacity of Zn foil, m_c is the specific gravimetric capacity (820 mAh g^{-1}) of Zn anode, ρ (7.14 g cm^{-3}) and l (100 μm) are the density and thickness of Zn foil, respectively. C_t =7.14 g cm^{-3} × 100 μm × 820 mAh g^{-1}= 58.5 mAh cm^{-2}. Thus, the DOD of Zn is 2.77%.

Energy density is calculated using the following equation[4]:

$$E = C_{PANI} \times m_{PANI} \times V / (m_{PANI} + m_{Zn})$$

C_{PANI} is the specific capacity of PANI, V is the discharge platform, m_{PANI} and m_{Zn} represent the mass of PANI (121.5 mg) and Zn (607 mg) respectively. Thus, the energy density of the Zn||PANI cell is calculated to be 19.2 Wh/kg.

Materials characterization

A field emission scanning electron microscope (SEM, Hitachi S-4800) was used to characterize morphology. X-ray diffraction (XRD) patterns were obtained on a Bruker D8 advance X-ray diffractometer with Cu-Kα radiation (=0.15418 nm). Optical surface

profilometry images were measured by an optical profilometer (Veeco, NT9300). The Fourier transform infrared (FTIR) (3000 Hyperion Microscope) was used to detect the presence of CB[6] on Zn foil. The conductivity of the electrolytes with different additive concentrations was obtained using a conductivity meter (Rex Electric Chemical, DDS-307A). In-situ optical microscope video and images were obtained from a YP510TR optical microscope (Suzhou Yueshi Precision Instrument Co. LTD). Galvanostatic Zn plating was conducted by an electrochemical workstation (CHI760E, Chenhua, Shanghai) at a constant current density of 5 mA cm^{-1} at a fixed time of 40 mins.

Computation methods

DFT calculation method: All calculations were implemented in Materials Studio with the DMol3 code. The Perdew-Burke-Ernzerhof (PBE) functional of the generalized gradient approximation (GGA) was used to calculate the exchange-correlation energy. The double numerical plus polarization (DNP) was chosen during the geometry optimization. Grimme's DFT-D method was employed to describe the van der Waals interactions. A 30Å vacuum layer was introduced to ensure enough region to prevent the interaction of adjacent layers. A Monkhorst-Pack k-mesh with a $3\times3\times1$ k-point grid was used for structural optimization, while $6\times6\times1$ for electronic structure calculations. The convergence tolerances of energy change, maximum force, and maximum displacement were set as 2×10^{-5} Ha, 0.004 Ha/Å, and 0.005 Å, respectively.

Molecular dynamics (MD) simulations: Dynamic simulations were performed using the

Gromacs 2021.7 software. A force field for the created CB[6] molecule and SO_4^{2-} ion was generated using ORCA. First, the simulation system was constructed using Packmol. For the $ZnSO_4$ system without CB[6], 200 Zn ions, 200 SO_4^{2-} ions, and 11078 water molecules were randomly placed in the box. For the system with CB[6] added, 3 CB[6] molecules, 200 Zn ions, 200 SO_4^{2-} ions, and 11078 water molecules were randomly placed in the box. Subsequently, both systems underwent 50,000 steps of energy minimization to eliminate any initial structural clashes. This was followed by 100 ps of NVT (constant Number of particles, Volume, and Temperature) equilibration and 100 ps of NPT (constant Number of particles, Pressure, and Temperature) equilibration. Finally, a 20 ns NPT production simulation was conducted. The simulation was carried out at a temperature of 298.15 K (25 degrees Celsius) and a pressure of one standard atmosphere.

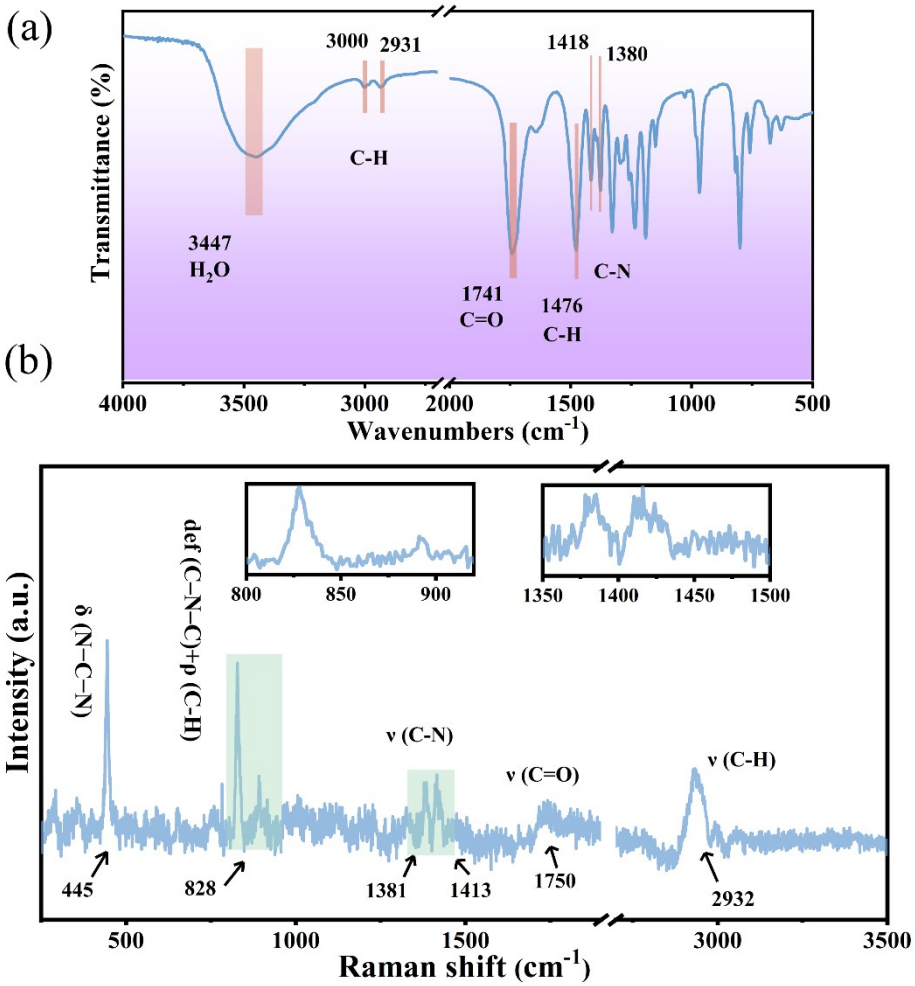

Fig. S1 Characterization of synthesized CB[6]: a. FTIR spectrogram of CB[6]; b. Raman spectrogram of CB[6][5]. In the FTIR spectrum, the peak for the C=O bond is at 1740 cm^{-1} and the peak for the C-N bond is at 1418 cm^{-1} and 1380 cm^{-1}. The Raman spectrum shows the peak of the C=O bond at 1750 cm^{-1} and the peak of the C-N bond at 1413 cm^{-1} and 1381 cm^{-1}.

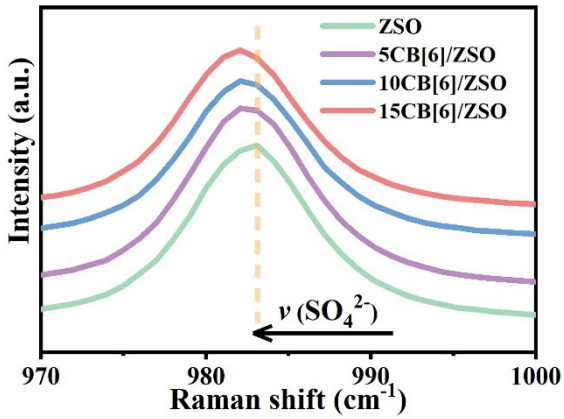

Fig. S2 Raman spectra of SO_4^{2-}stretching vibration in 1M ZSO with different CB[6] concentrations.

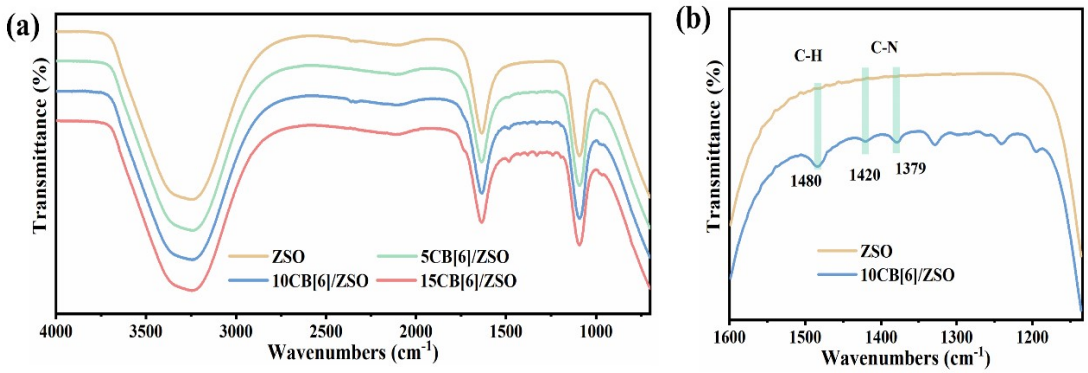

Fig. S3 FTIR spectra of ZSO, 5 mM CB[6]/ZSO, 10 mM CB[6]/ZSO and 15 mM CB[6]/ZSO.

As shown in Fig. S3, the FTIR spectra compare the characteristic peak changes of pure ZSO electrolyte and CB[6]/ZSO electrolyte with different concentrations of CB[6]. Compared with the ZSO electrolyte, the characteristic peak (C-N) of CB[6] can be observed in the FTIR spectrum of CB[6]/ZSO, indicating that CB[6] has been successfully introduced into ZSO electrolyte.

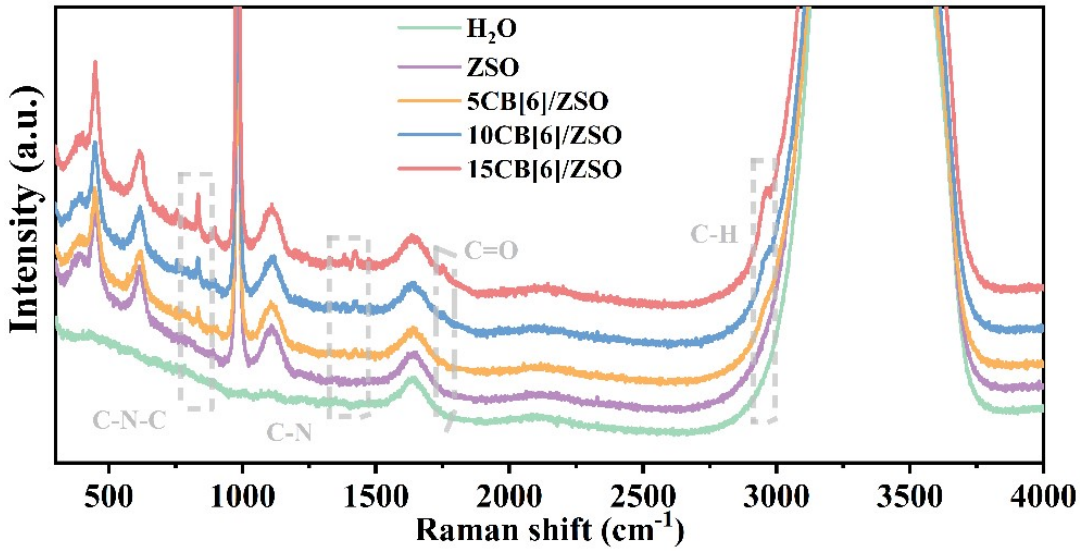

Fig. S4 Raman spectra of H_2O, ZSO, 5 mM CB[6]/ZSO, 10 mM CB[6]/ZSO and 15 mM CB[6]/ZSO. The C=O (1746 cm^{-1}) bond shift also suggests the involvement of CB[6] in the solvated structure of Zn^{2+}.

To further illustrate this point, we also characterized the electrolyte mentioned above by Raman spectroscopy. As shown in Figure S4, characteristic peaks such as C=O and C-N belonging to CB[6] also appear in the Raman spectrum of CB[6]/ZSO. In summary, both FTIR (Fig. S3) and Raman spectra (Fig. S4) of CB[6]/ZSO indicate that the CB[6] has been successfully introduced into the ZSO electrolyte.

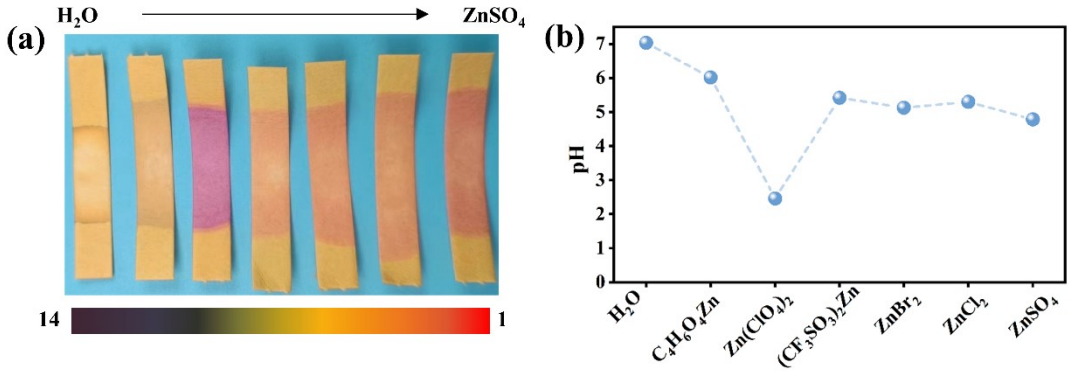

Fig. S5 Measurement of pH of different solutions using pH paper (a) and pH meter (b). As shown in Fig. S5a, the pH of the solutions is qualitatively compared using pH paper (from left to right, it is H_2O, $C_4H_6O_4Zn$, $Zn(ClO_4)_2$, $(CF_3SO_3)_2Zn$, $ZnBr_2$, $ZnCl_2$ and $ZnSO_4$ in order). By comparing the depth of colors, it can be found that $Zn(ClO_4)_2$ has the lowest pH and H_2O has the highest pH. Furthermore, pH meter is used for their quantitative characterization. Similarly, H_2O has the highest pH, followed by $C_4H_6O_4Zn$, with $Zn(ClO_4)_2$ having the lowest pH. The pH values of $(CF_3SO_3)_2Zn$, $ZnBr_2$, $ZnCl_2$, and $ZnSO_4$ are not significantly different. As shown in Fig. S5b of the manuscript, the solubility of CB[6] in these seven solutions increases sequentially from left to right. From the perspective of pH, the solubility of CB[6] does not increase with decreasing pH.

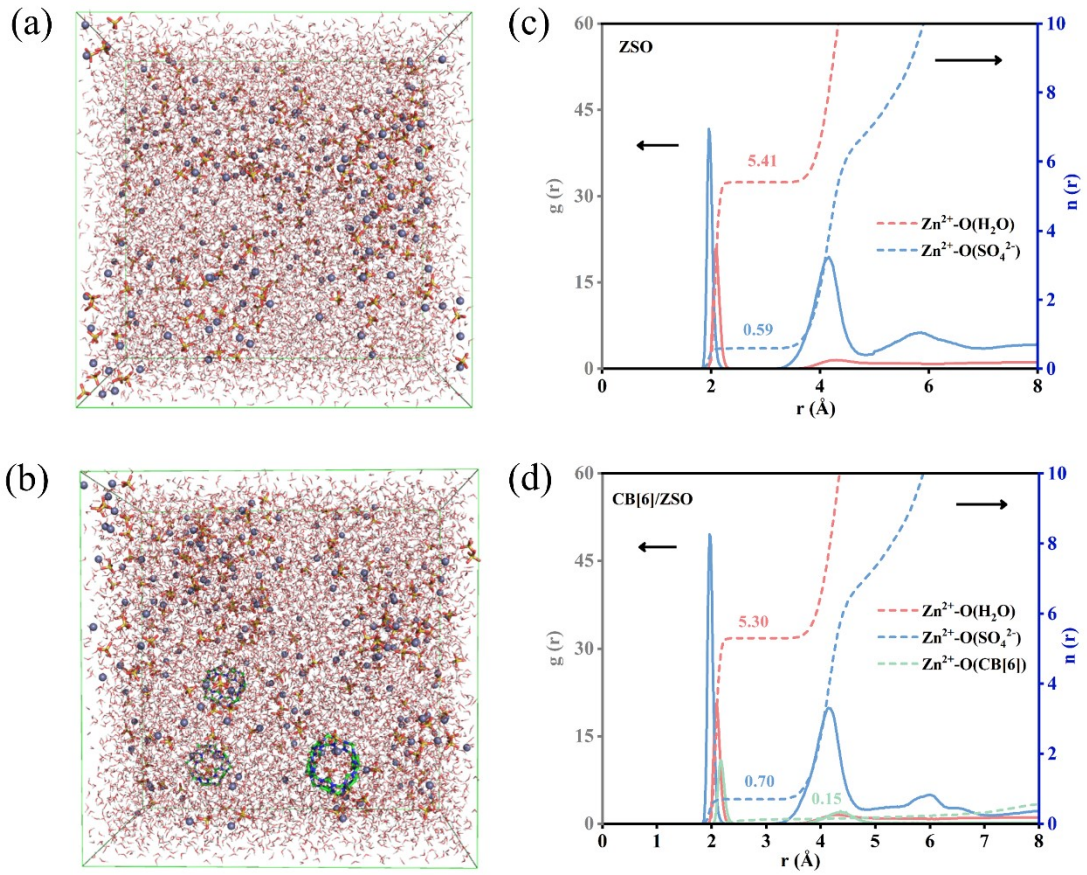

Fig. S6 The 3D snapshot of ZSO (a) and CB[6]/ZSO (b) electrolytes, The radial distribution functions and coordination numbers of Zn^{2+}-O obtained from MD simulations in (c) ZSO and (d) CB[6]/ZSO electrolytes. In conventional ZSO electrolyte, the average coordination number (CN) of H_2O and SO_4^{2-} to Zn^{2+} are 5.41 and 0.59, respectively. After the introduction of CB[6] additive, the coordination number of Zn^{2+}-O (H_2O) decreased to 5.30, demonstrating that CB[6] molecules can enter the inner solvation shell. In the CB[6]/ZSO electrolyte, the average coordination number for Zn^{2+}-O (CB[6]) coordination is 0.15, indicating the reconstruction of the solvation structure[6].

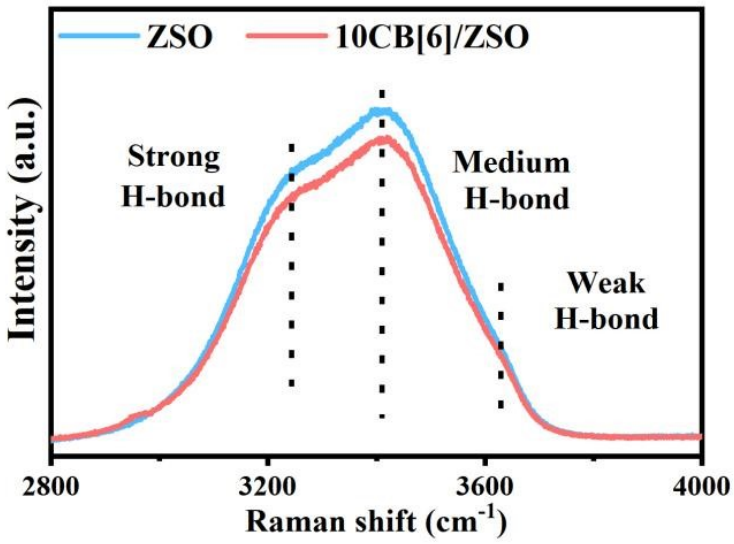

Fig. S7 O-H bending part from the Raman curves of 1M ZSO with 10mM CB[6] addition.

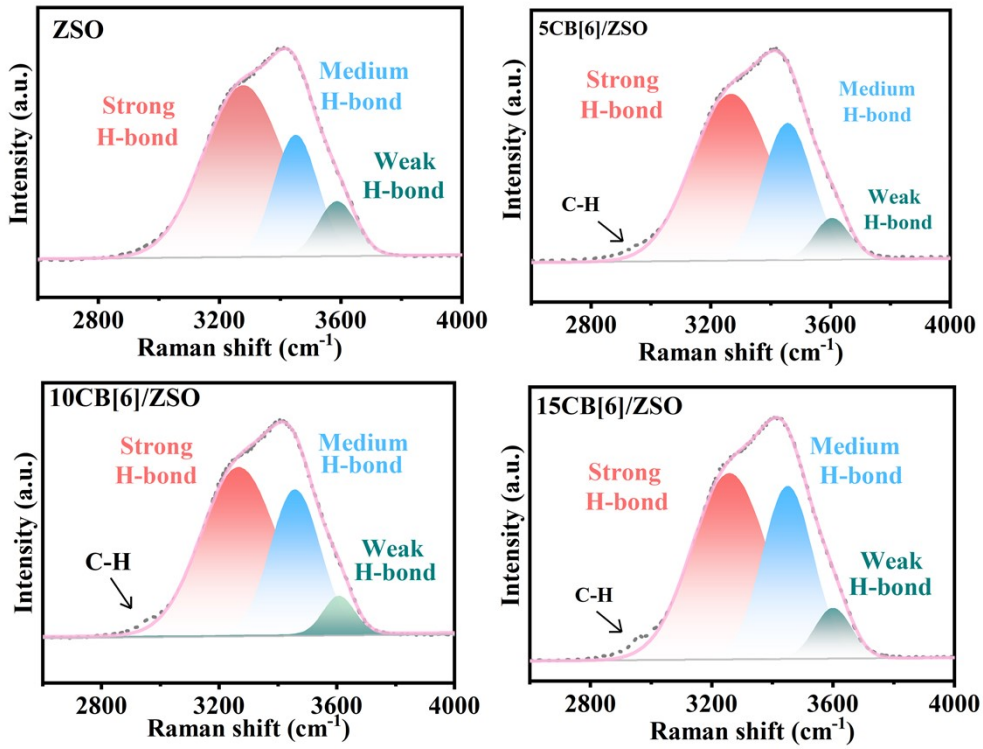

Fig. S8 The Raman of ZSO, 5 mM CB[6]/ZSO, 10 mM CB[6]/ZSO and 15 mM CB[6]/ZSO electrolytes were fitted with three peaks representing the O-H stretching vibration of H_2O in weak, medium, strong H-bond state.

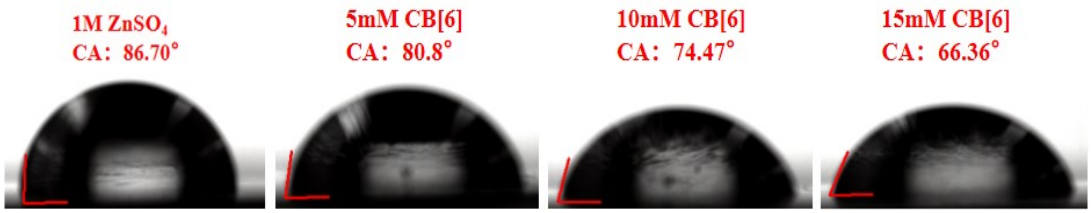

Fig. S9 Contact angle measurement of 1 M ZSO and 1 M ZSO/CB[6] electrolytes on Zn electrode.

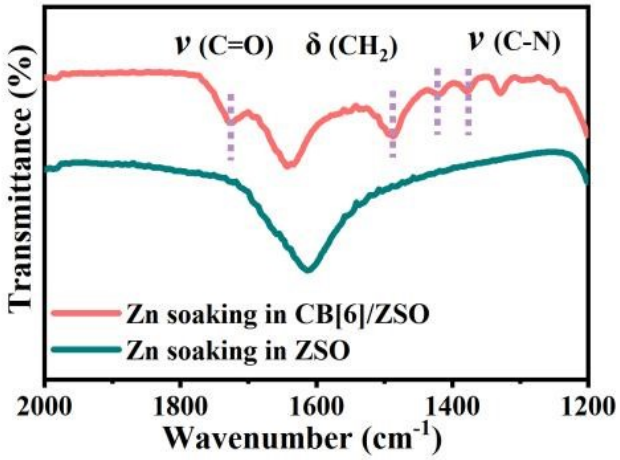

Fig. S10 ATR-FTIR spectra of Zn foil soaking in ZSO and Zn soaking in CB[6]/ZSO electrolyte.

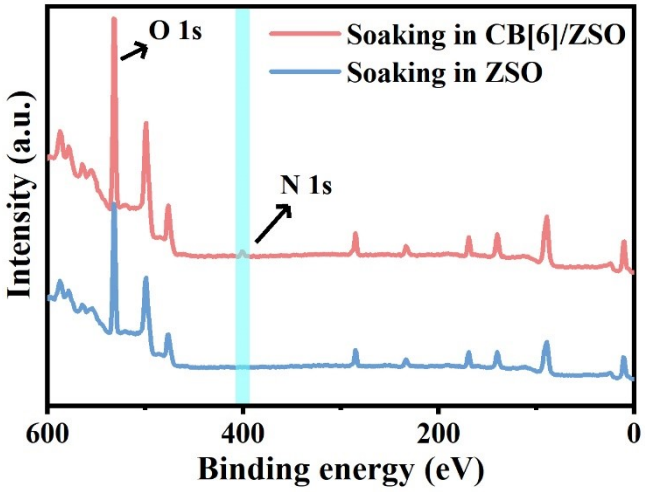

Fig. S11 XPS surveys of the Zn anode before and after immersing into the ZSO and CB[6]/ZSO solution (full spectrum).

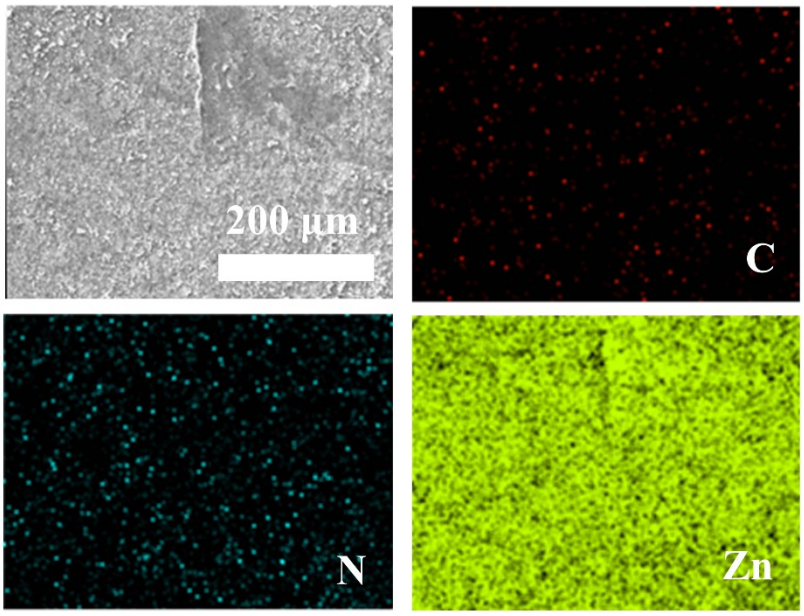

Fig. S12 EDS image of zinc foil after immersion in CB[6]/ZSO electrolyte.

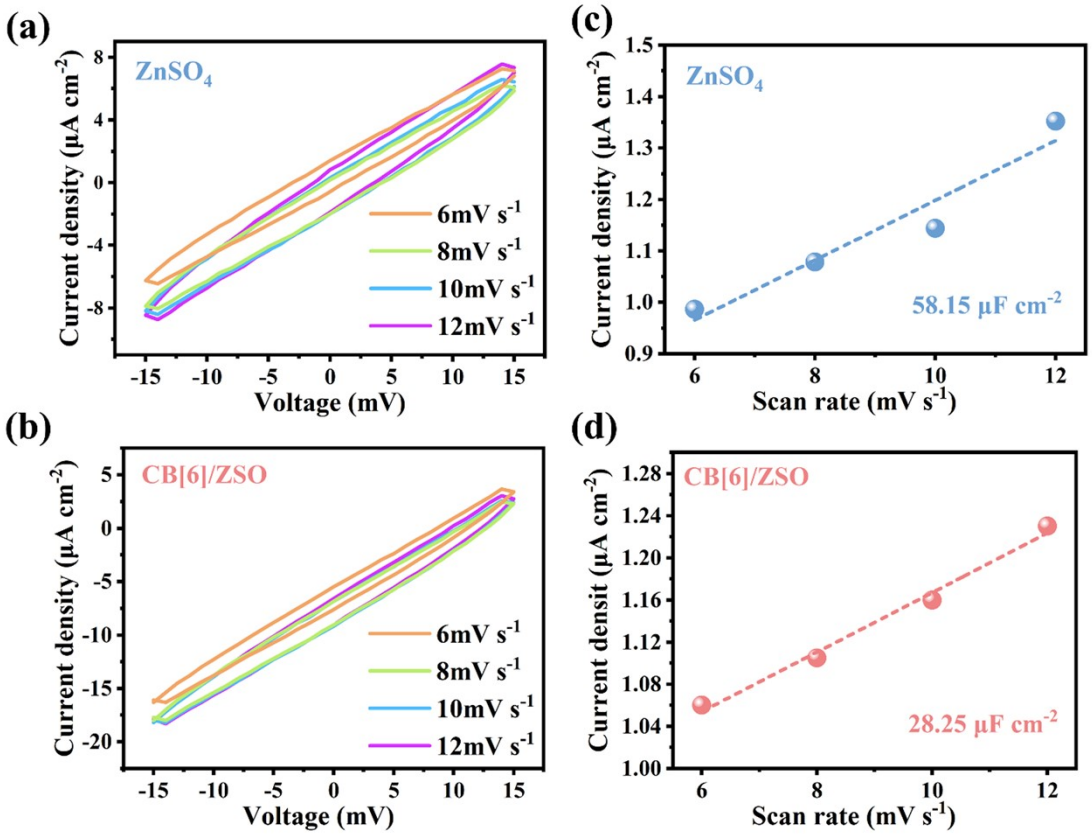

Fig. S13 Electric double layer capacitance (EDLC) measurements for Zn substrates in 1 M ZSO electrolytes with and without CB[6] additive. CV curves for the Zn||Zn symmetric cells in the voltage range of -15 mV to 15 mV under various scanning rates in the electrolyte without (a) or with (b) CB[6] additive. The plots of capacitive currents versus scan rates for the cell cycled in the electrolyte without (c) or with (d) CB[6] additive. The electric double-layer capacitance (EDLC) was calculated through the equation of $C=i_c/v$, where C is the capacitance, i_c is the double layer current, v is the scan rate.

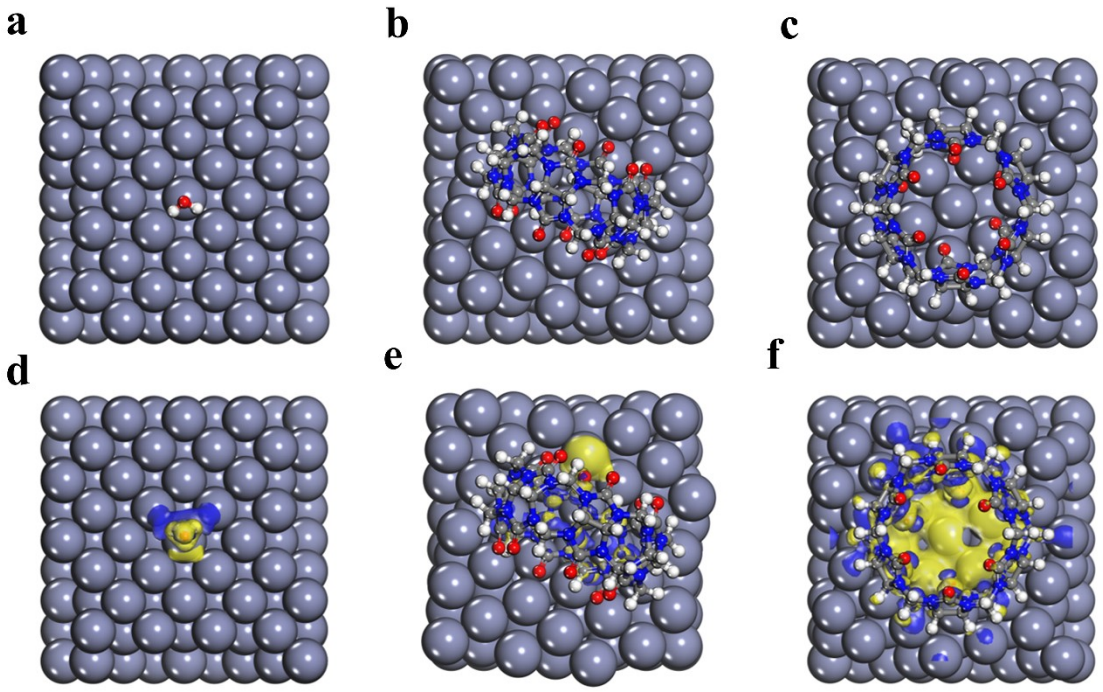

Fig. S14 Top view of different adsorption states of water and CB[6] molecules on Zn surface, respectively (a-c). Charge density difference of Zn (002) plane with H_2O and CB[6] adsorbates (d-f).

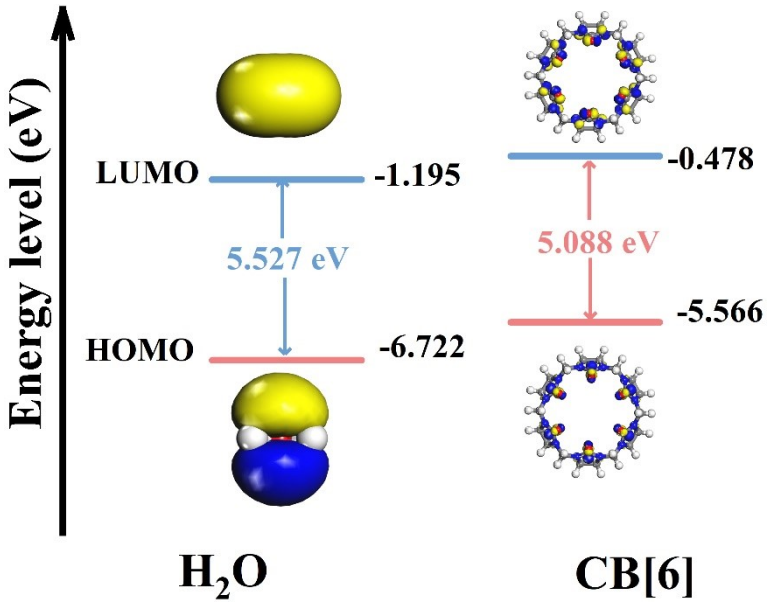

Fig. S15 HOMO/LUMO energy levels of H_2O and CB[6] molecules.

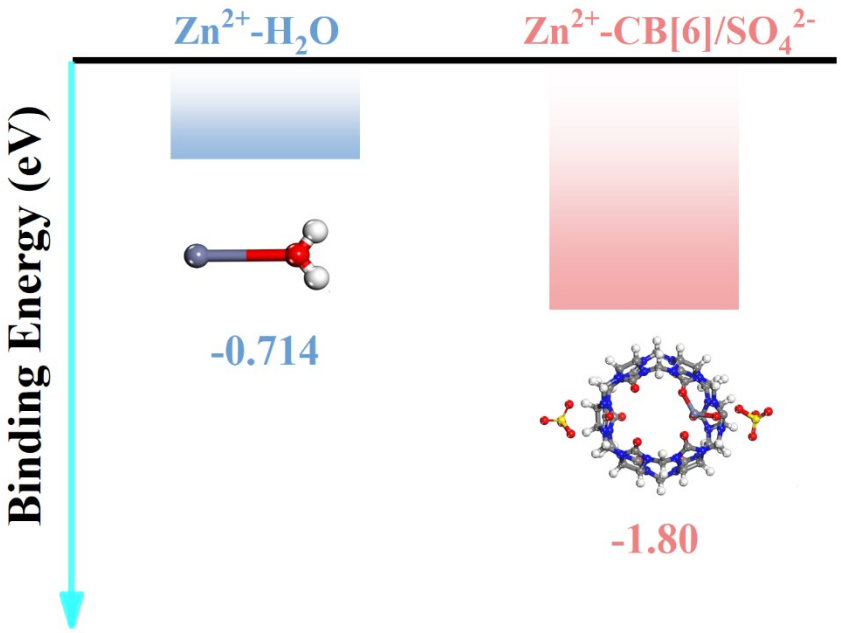

Fig. S16 Binding energy of H_2O and CB[6]/SO_4^{2-} complex to Zn^{2+}

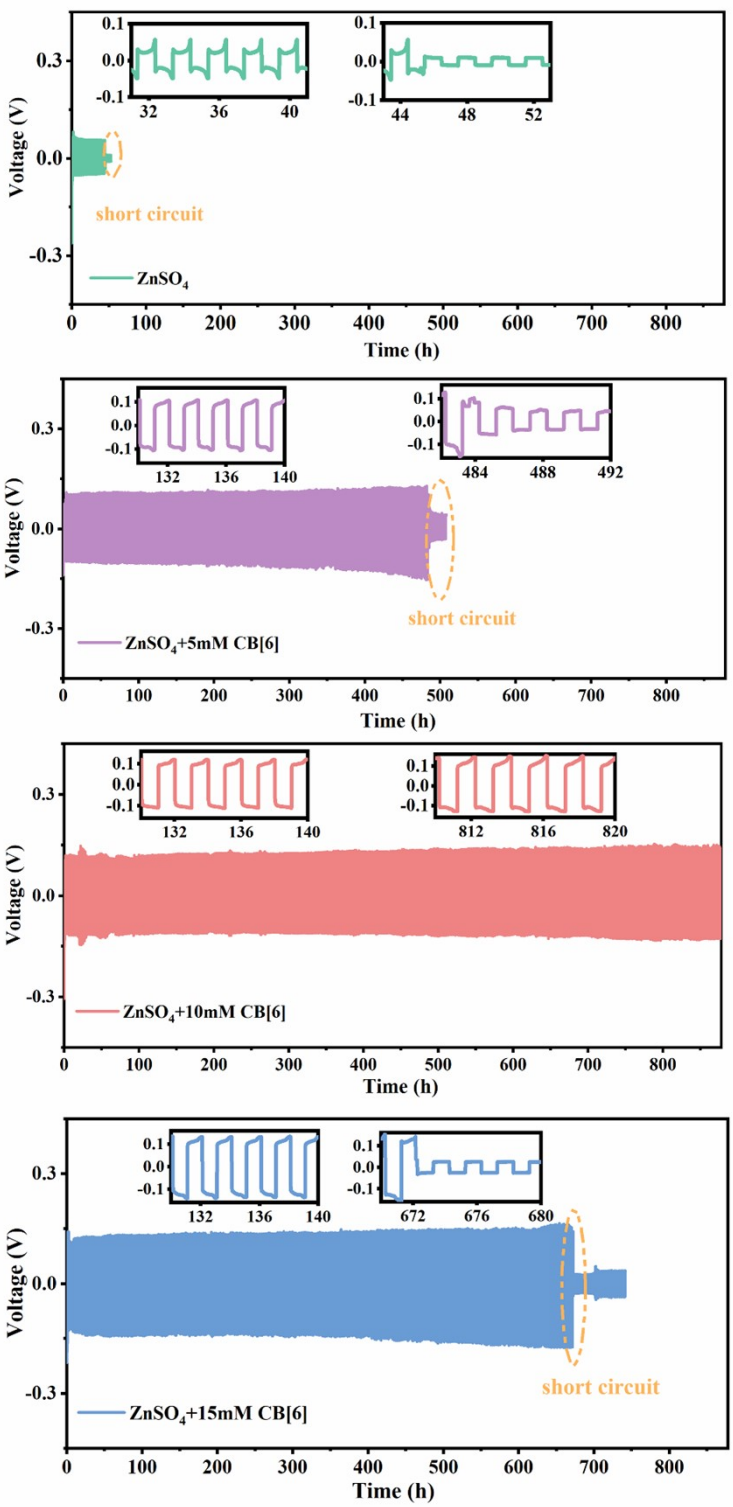

Fig. S17 Long-term galvanostatic cycling performances of Zn||Zn cells in varied CB[6]-containing electrolytes at 5 mA cm^{-2}, 5 mAh cm^{-2}. By comparing the long cycles of symmetric cells, it is found that the deposition/stripping of Zn anode is reversibly better when the concentration of CB[6] additive is 10 mM.

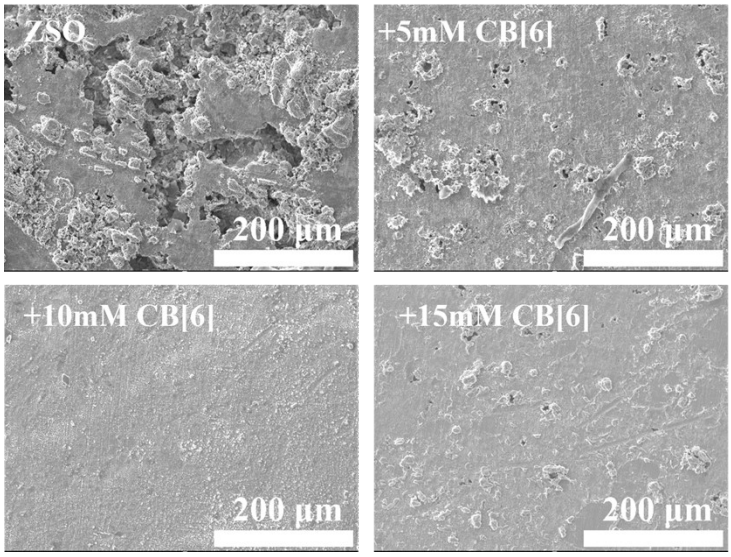

Fig. S18 SEM images of Zn anodes corresponding to different concentrations of additives after 50 h of cycling at a current density of 2 mA cm^{-2} and areal capacity of 2 mAh cm^{-2}. The SEM image of the Zn anode after cycling also shows that the surface of the Zn anode is flatter at a concentration of 10 mM CB[6] additive.

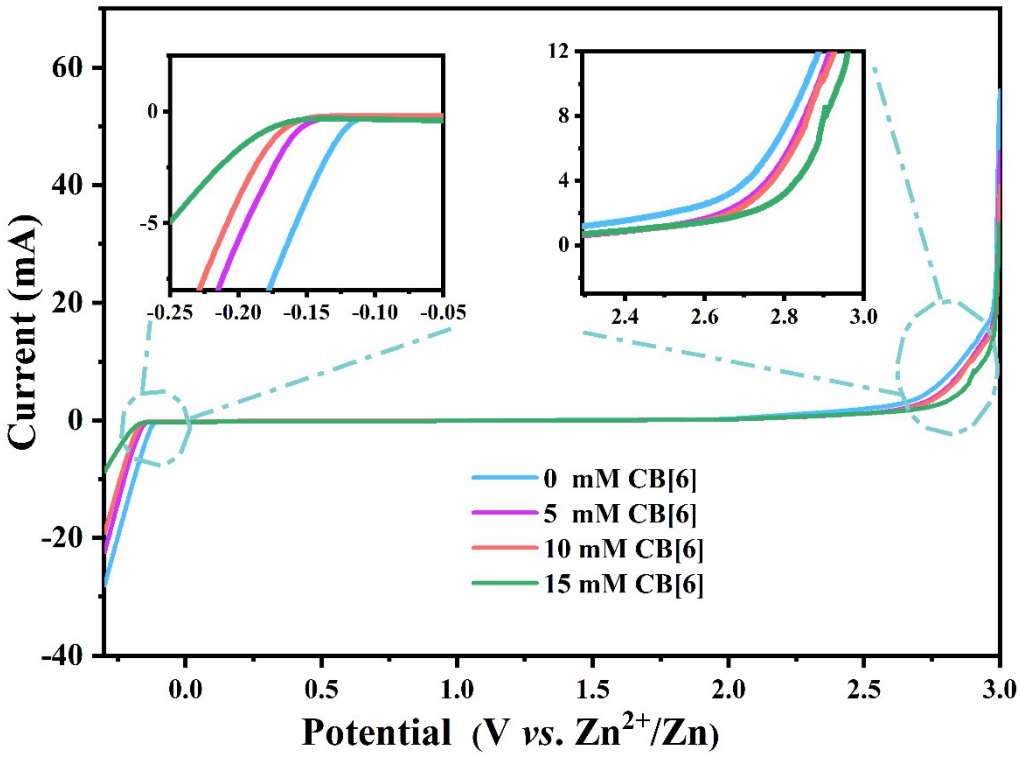

Fig. S19 Linear scan voltammetry (LSV) curves in 1 M $ZnSO_4$ without and with 5 mM, 10 mM and 15 mM CB[6] at a scan rate of 1 mV s^{-1}.

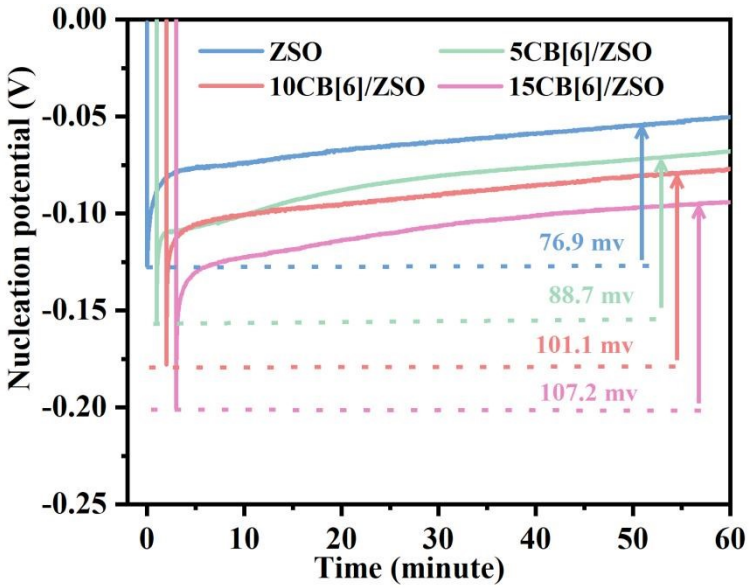

Fig. S20 Nucleation overpotentials of symmetric cells corresponding to different concentrations of CB[6] additives.

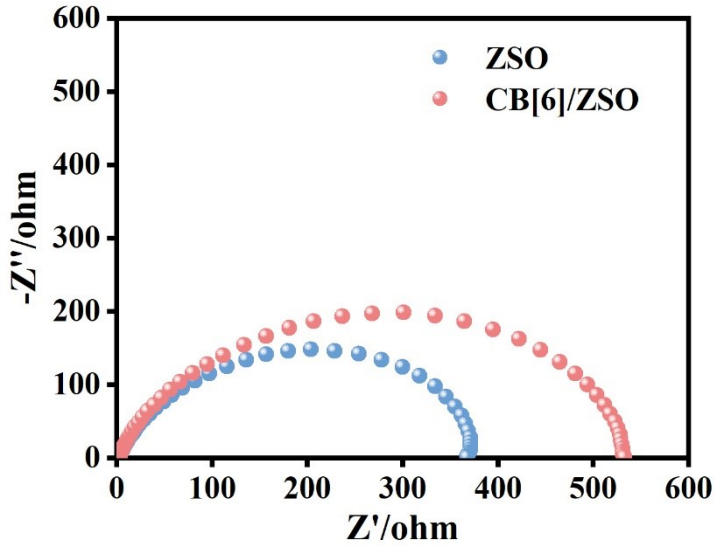

Fig. S21 EIS spectra of symmetric cells corresponding to different electrolytes.

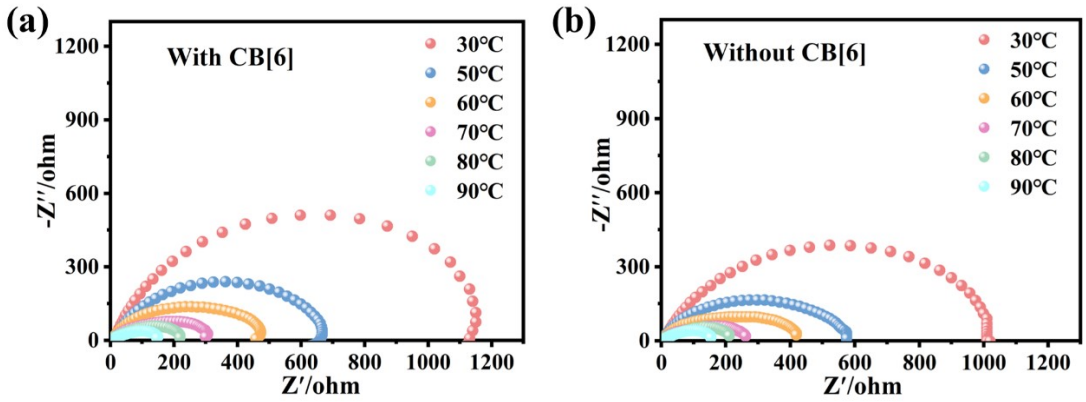

Fig. S22 EIS spectra of symmetric cells with (a) and without (b) CB[6] additives at different temperature conditions.

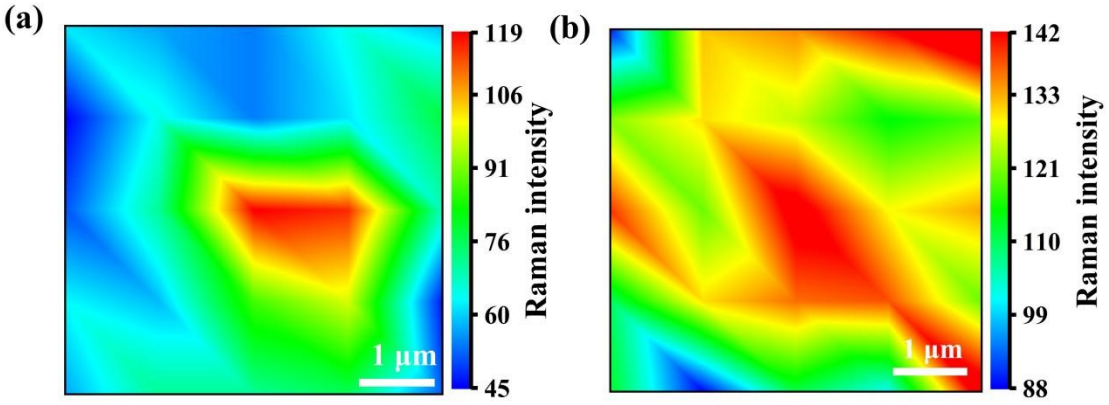

Fig. S23 Raman mapping of surfaces for 10 mM CB[6]/ZSO (a) and ZSO (b) after 50 cycles.

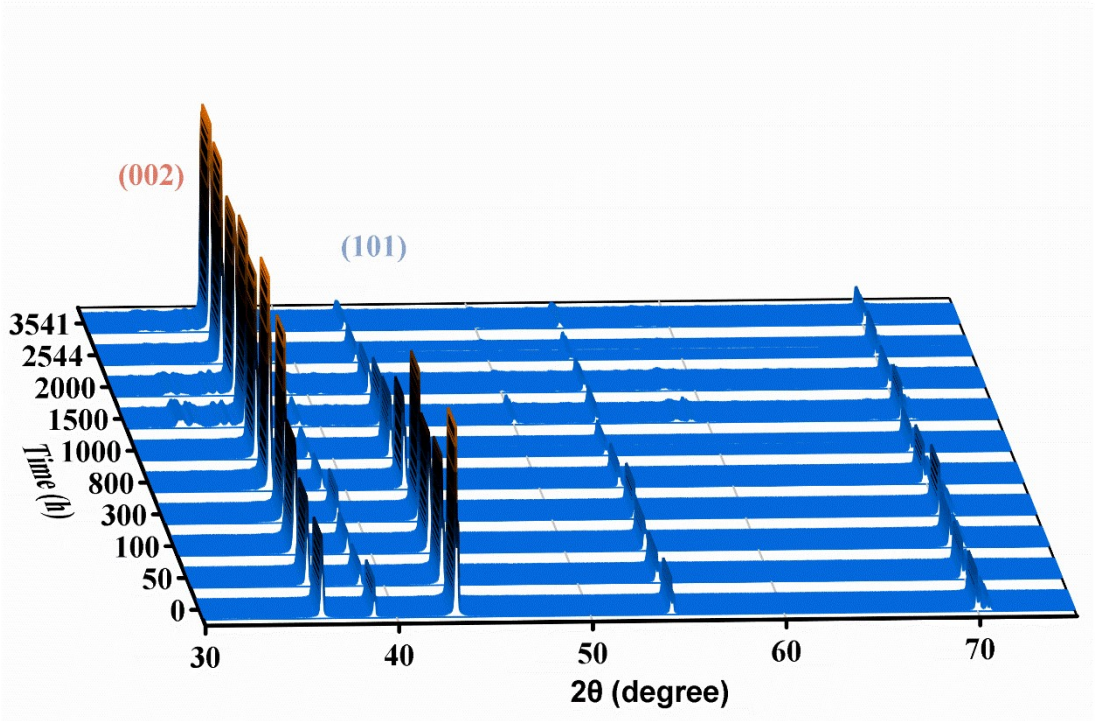

Fig. S24 XRD images.

Table S1. Intensity obtained from textured sample I(hkl) and the intensity of the standard oriented sample I_0(hkl) of Zn anodes.

Intensity	002	100	101	102	103	110
I_0	53	40	100	28	25	21
I-0h	186064.3	88396.1	430807.9	85240.6	94024.6	36183.8
I-50h	202720.8	52723.7	293884.3	72223.7	88703.7	25211.8
I-100h	262394.6	51467.3	274684.0	73130.3	81147.3	33421.6
I-300h	427963.2	78350.1	343422.8	83433.3	118001.7	35855.7
I-800h	480309.7	42117.5	213068.1	56725.6	91065.4	19662.3
I-1000h	598518.2	45530.9	207721.0	56956.7	89788.3	19243.2
I-1500h	437681.7	24634.6	112140.7	42694.1	83042.6	14649.8
I-2000h	408545.1	15603.6	71728.9	32796.5	54158.8	10214.1
I-2544h	459036.7	11427.6	43051.4	20222.9	60436.4	4751.9
I-3541h	472122.4	7766.7	24718.2	15545.7	43225.0	4715.5

The relative texture coefficients (RTCs) of each Zn lattice plane were calculated using the following formula,

$$RCT(hkl) = \frac{I(hkl)/I0(hkl)}{\sum(I(hkl)/I0(hkl))}$$

where $I_{(hkl)}$ is the intensity obtained from the textured sample, and $I_{0(hkl)}$ is the intensity of the standard-oriented sample[7].

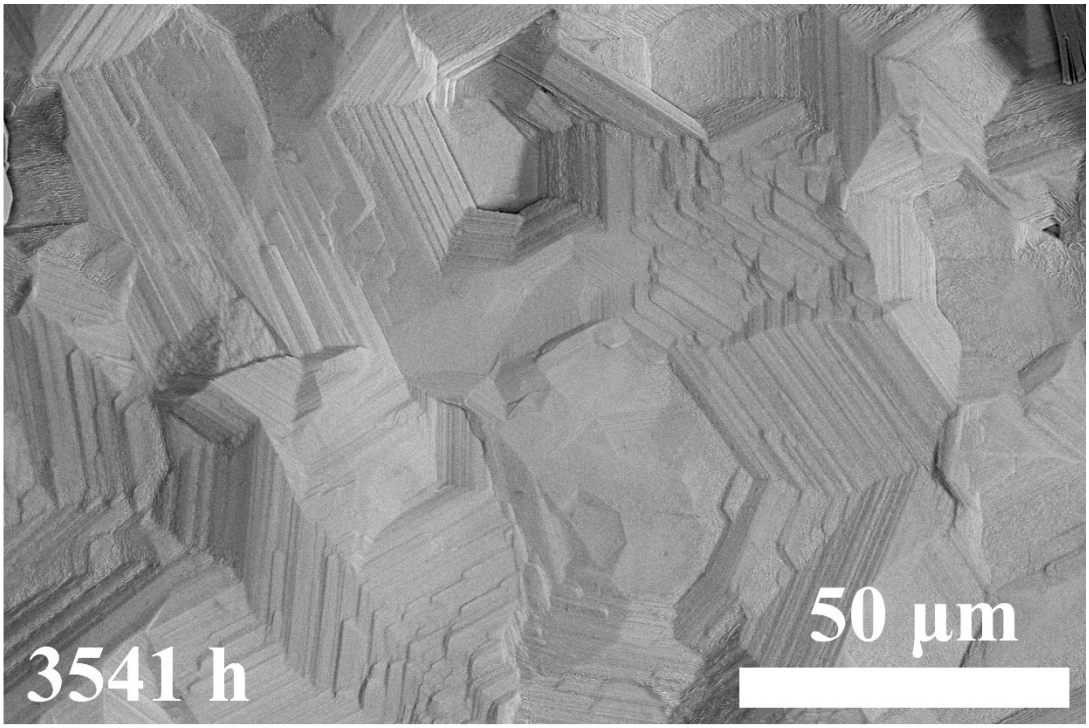

Fig. S25 SEM image of zinc anode in CB[6]/ZSO electrolyte after 3541 hours.

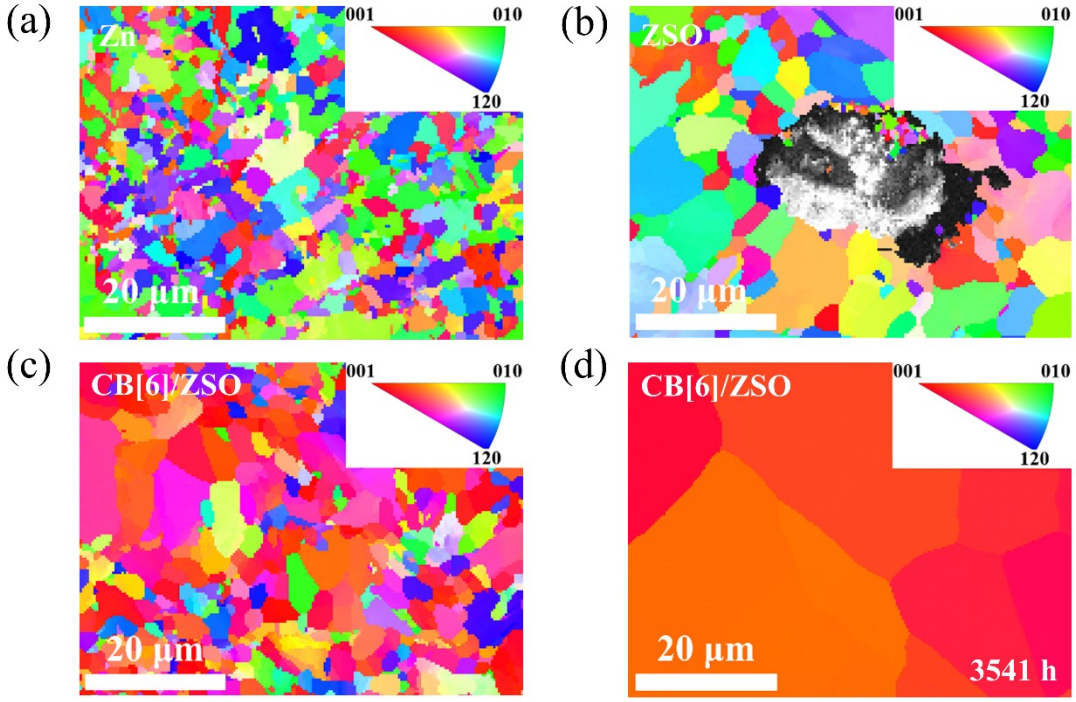

Fig. S26 EBSD orientation distribution map of Zn deposited on Zn substrate after argon ion polishing. (a) fresh Zn, cycled Zn electrodes with (b) ZSO and (c-d) CB[6]/ZSO electrolyte. Fig. S26 show the inverse pole figure (IPF) mapping results of the pole pieces in the Z directions. For the fresh Zn, there are multiple grains with various crystal orientations exposed on its surface. However, after 100 cycles (1 mA cm^{-2}/1 mAh cm^{-2}) in ZSO, the indexing rate decreases and unrecognisable grains appear. This may be assigned to the large surface residual stress caused by by-products coverage. Conversely, the case in CB[6]/ZSO shows discernible texture information with a much higher indexing rate, identifying the wellpreserved crystalline structure and less parasitic reactions in CB[6]/ZSO.

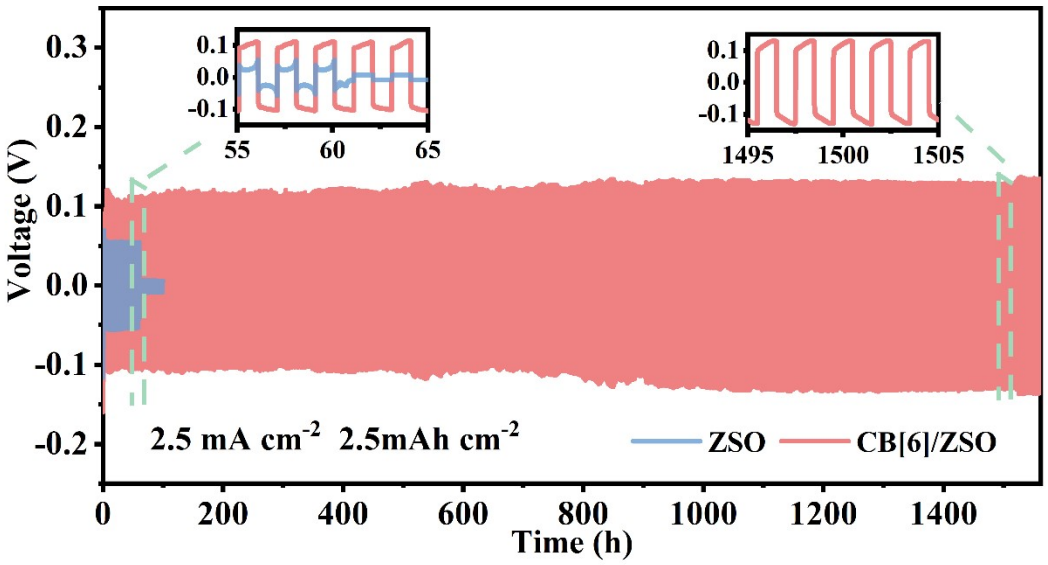

Fig. S27 Cycling stability of Zn||Zn symmetric cells in ZSO and 10 mM CB[6]/ZSO at a current density of 2.5 mA cm^{-2} and a Zn capacity of 2.5 mAh cm^{-2}.

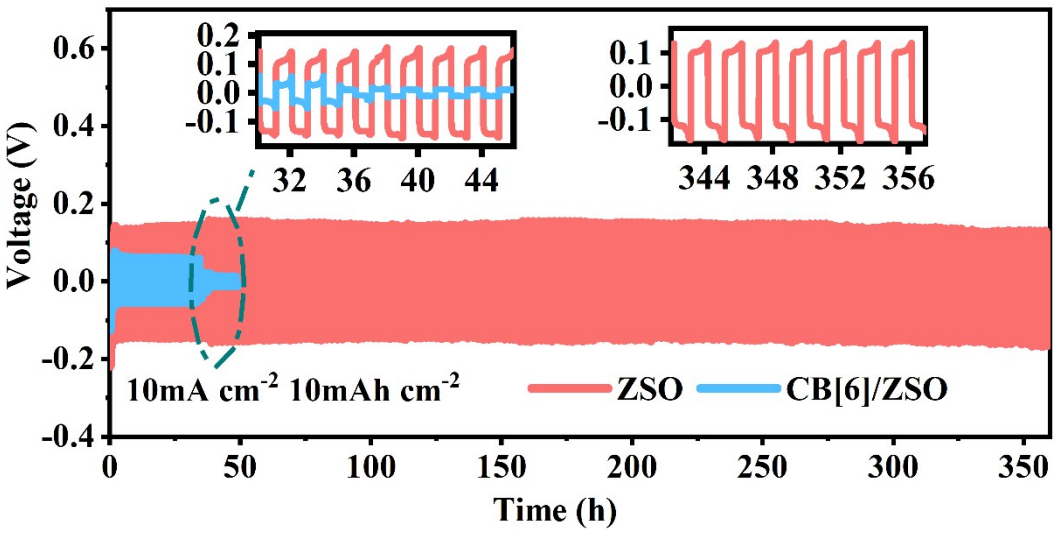

Fig. S28 Cycling stability of Zn||Zn symmetric cells in ZSO and 10 mM CB[6]/ZSO at a current density of 10 mA cm^{-2} and a Zn capacity of 10 mAh cm^{-2}.

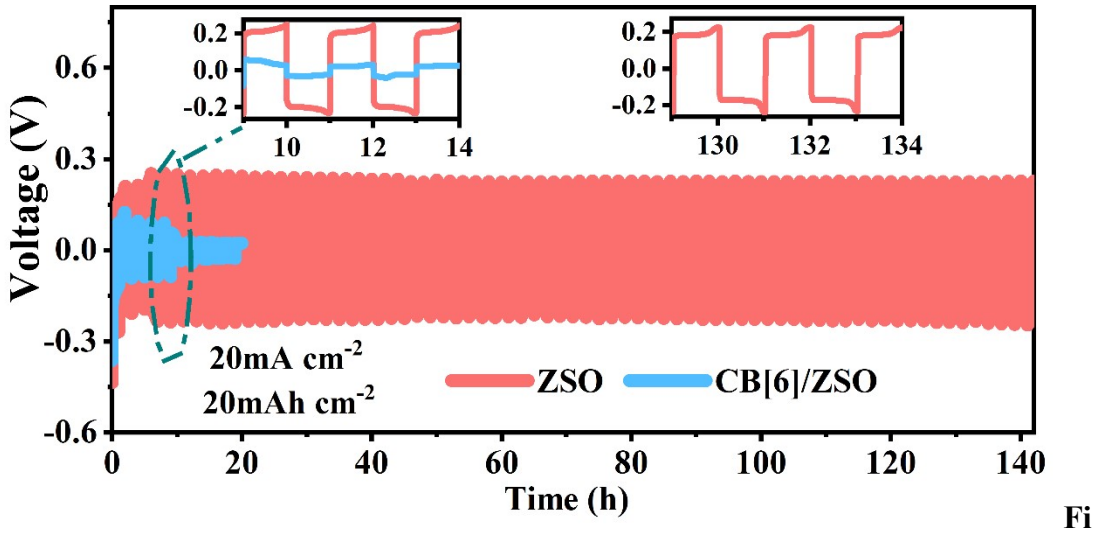

Fi

g. S29 Cycling stability of Zn||Zn symmetric cells in ZSO and 10 mM CB[6]/ZSO at a current density of 20 mA cm^{-2} and a Zn capacity of 20 mAh cm^{-2}.

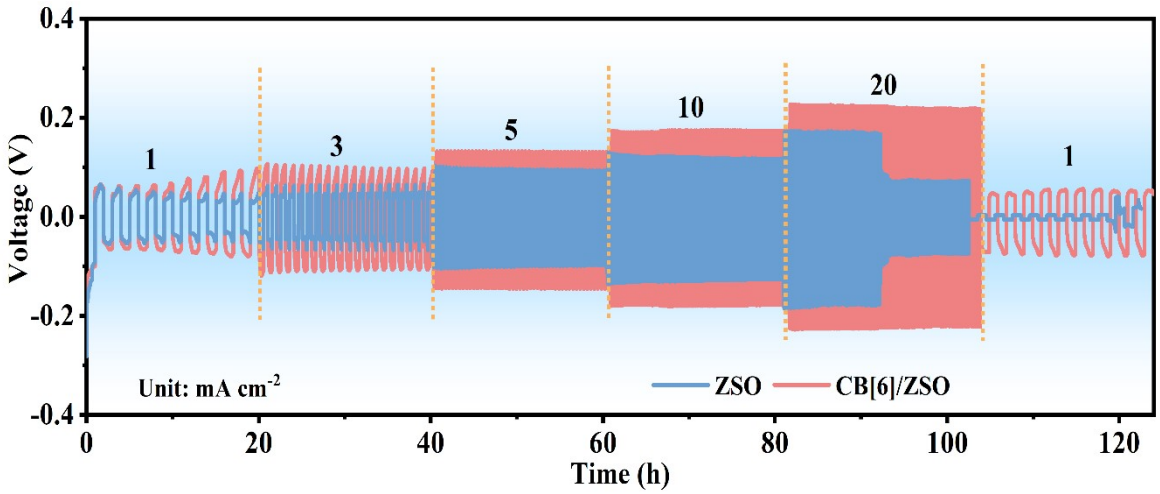

Fig. S30 Rate performance of Zn-Zn symmetric cells with and without CB[6] additive at the same cycle time.

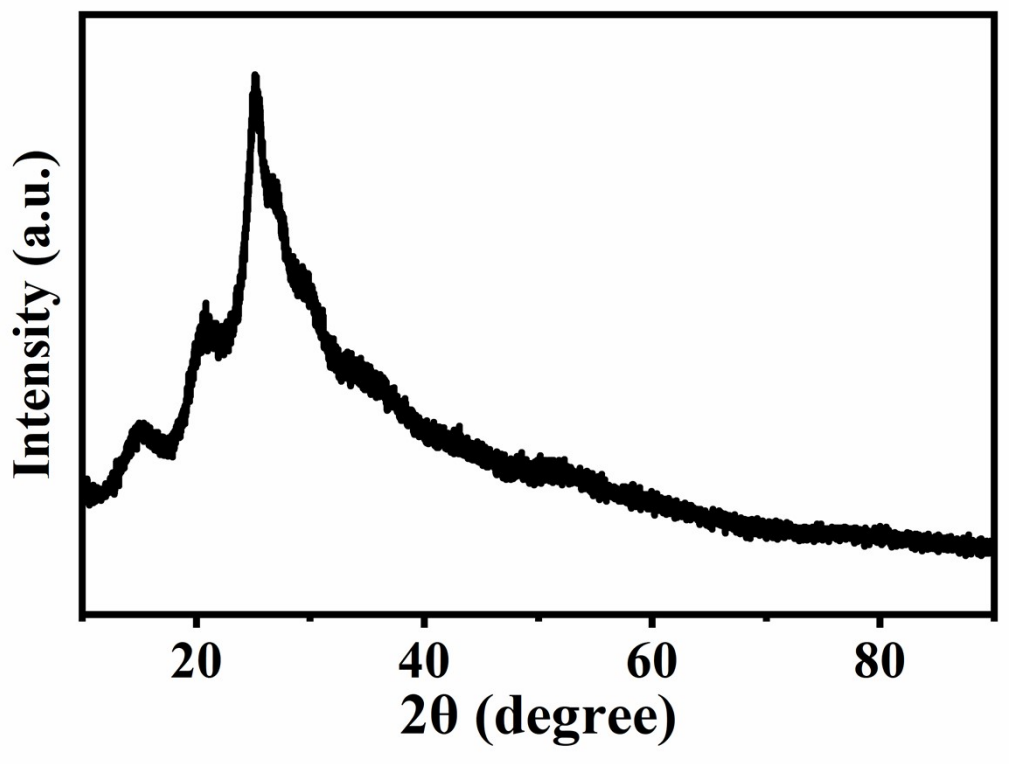

Fig. S31 XRD characterization images of PANI.

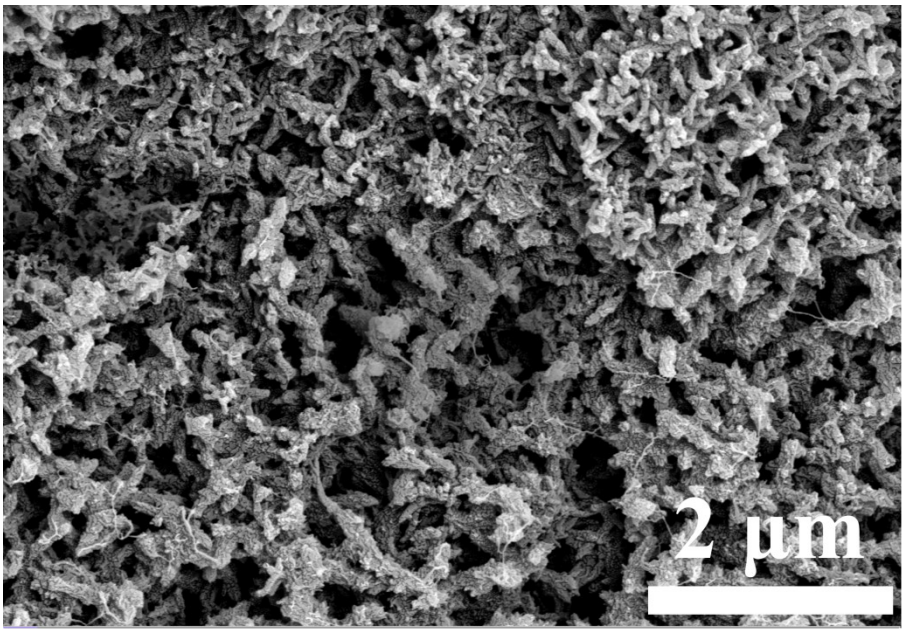

Fig. S32 SEM image of PANI at high magnification.

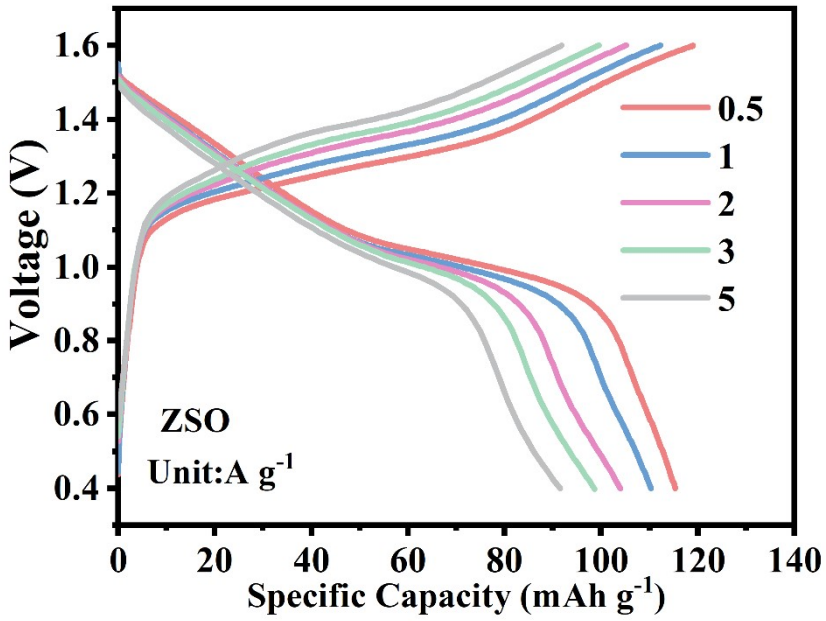

Fig. S33 The charge-discharge curves of Zn||PANI batteries with ZSO electrolytes under different current densities.

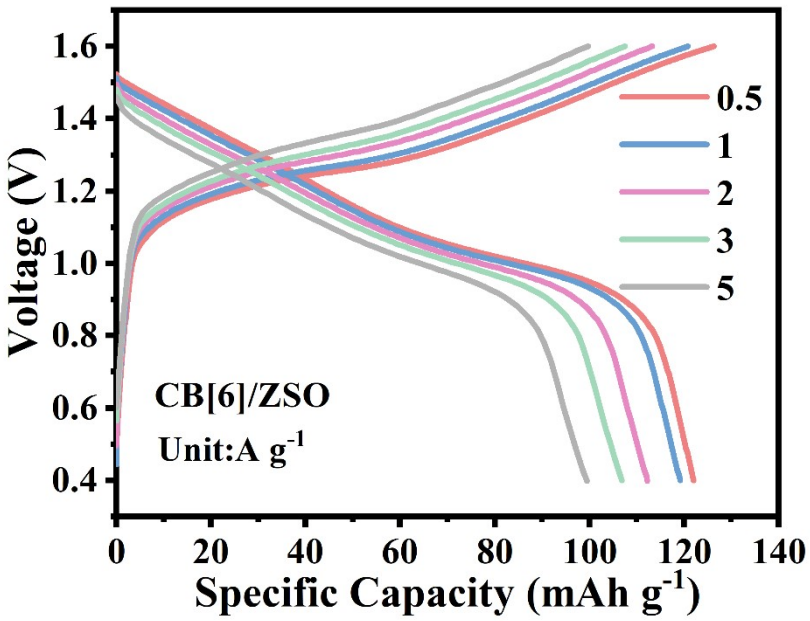

Fig. S34 The charge-discharge curves of Zn||PANI batteries with 10 mM CB[6]/ZSO electrolytes under different current densities.

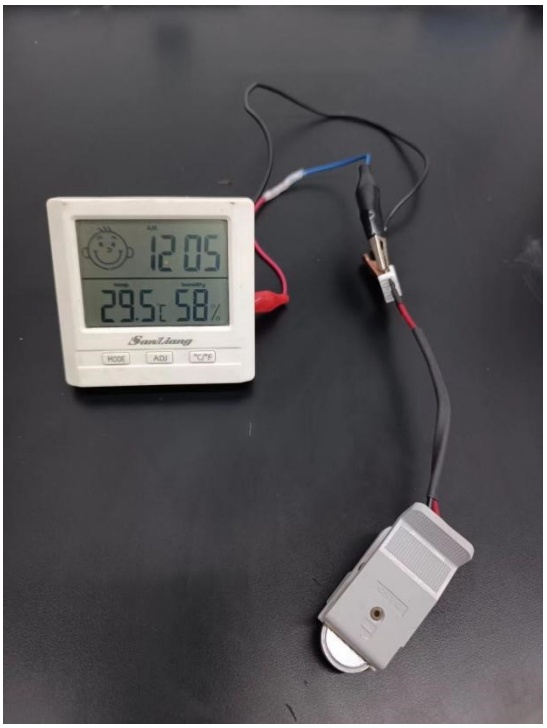

Fig. S35 Photograph of a Zn||PANI full cell making an electronic display work properly.

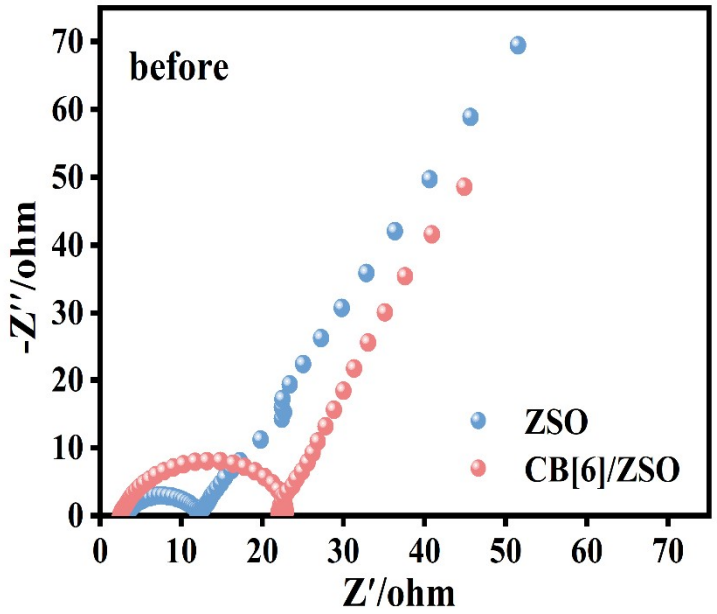

Fig. S36 EIS spectra of symmetric cells with and without CB[6] additives before cycling.

Notes and references

[1] a)S. Y. Jon, N. Selvapalam, D. H. Oh, J.-K. Kang, S.-Y. Kim, Y. J. Jeon, J. W. Lee, K. Kim, *Journal of the American Chemical Society* **2003**, 125, 10186; b)D. Bardelang, K. A. Udachin, D. M. Leek, J. C. Margeson, G. Chan, C. I. Ratcliffe, J. A. Ripmeester, *Crystal Growth & Design* **2011**, 11, 5598.

[2] S.-J. Zhang, J. Hao, Y. Zhu, H. Li, Z. Lin, S.-Z. Qiao, *Angewandte Chemie International Edition* **2023**, 62, e202301570.

[3] H. Wang, W. Ye, B. Yin, K. Wang, M. S. Riaz, B. B. Xie, Y. Zhong, Y. Hu, *Angewandte Chemie International Edition* 2023, 62, e202218872.

[4] a)X. Li, X. Jin, Y. Wang, X. Zhang, D. Li, J. Wang, M. Yuan, J. Liu, Y. Zhao, *Advanced Functional Materials 2023*, 2314060; b)H. Yang, R. Zhu, Y. Yang, Z. Lu, Z. Chang, P. He, C. Zhu, S. Kitano, Y. Aoki, H. Habazaki, H. Zhou, *Energy & Environmental Science* 2023, 16, 2133.

[5] a)X. Xie, X. Li, H. Luo, H. Lu, F. Chen, W. Li, *The Journal of Physical Chemistry B* **2016**, 120, 4131; b)X. Li, X. Xie, H. Luo, L. Li, Z. Li, Z. Xue, W. Li, *Journal of Colloid and Interface Science* **2017**, 498, 31.

[6] Q. Guo, G. Teri, W. Mo, J. Huang, F. Liu, M. Ye, D. Fu, *Energy & Environmental Science* 2024, 17, 2888.

[7] a)Y. Qin, H. Li, C. Han, F. Mo, X. Wang, *Advanced Materials* **2022**, 34; b)M. Zhou, S. Guo, J. Li, X. Luo, Z. Liu, T. Zhang, X. Cao, M. Long, B. Lu, A. Pan, G. Fang, J. Zhou, S. Liang, *Advanced Materials* **2021**, 33, 2100187 .